COMPDYN 2013
4th ECCOMAS Thematic Conference on
Computational Methods in Structural Dynamics and Earthquake Engineering
M. Papadrakakis, V. Papadopoulos, V. Plevris (eds.)
Kos Island, Greece, 12–14 June 2013

AN OUTLOOK INTO TIME-DEPENDENT AFTERSHOCK VULNERABILITY ASSESSMENT

Hossein Ebrahimian[1], Fatemeh Jalayer[1], Domenico Asprone[1], Anna M. Lombardi[2], Warner Marzocchi[2], Andrea Prota[1], and Gaetano Manfredi[1]

[1] Department of Structures for Engineering and Architecture, University of Naples Federico II, Naples, Italy
e-mail: ebrahimian.hossein@unina.it, fatemeh.jalayer@unina.it

[2] Istituto Nazionale di Geofisica e Vulcanologia (INGV), Rome, Italy

Keywords: Aftershock hazard, Time-dependent vulnerability assessment, Daily rate of exceedance, Sequential cloud analysis, Modified Omori model, ETAS model.

Abstract. *Operative seismic aftershock risk forecasting is particularly useful as support for rapid decision-making in the presence of an ongoing aftershock sequence. Arguably, an operative forecasting framework can be built on the basis of adaptive time-dependent seismic aftershock risk assessment. In such a context, the fragility curves represent the progressive state of damage in a structure. Focusing on adaptive time- and event-dependent fragility assessment, this work explores various issues related to probability-based performance assessment in the immediate post main-shock environment. A fragility curve is expressed herein as the daily probability of (first-excursion) exceeding of a prescribed limit states given the first-mode spectral acceleration. A time-dependent structural performance variable, defined as the ratio of residual demand to residual capacity, is adopted in order to measure the cumulative damage in the structure. The sequence of event-dependent fragility curves are calculated by evolutionary linear logarithmic regression of the structural performance variable versus spectral acceleration, called herein as the sequential cloud method. It is demonstrated that the aftershock recurrence model used to estimate the daily number events of interest significantly affects the resulting fragility curves. Two alternative aftershock occurrence models based on the ETAS model and the modified Omori are studied herein. The sequence of daily fragility curves for a given limit state are finally integrated together with daily aftershock hazard curves (based on above-mentioned aftershock models) in order to calculate the daily aftershock risk. As a numerical example, the daily aftershock risk is calculated for the L'Aquila 2009 aftershock sequence (central Italy). An equivalent single-degree-of-freedom structure with cyclic strength and stiffness degradation is used in order to evaluate the progressive damage caused by the sequence of aftershock events.*

1 INTRODUCTION

The first few days after the occurrence of a strong earthquake are crucial in decision-making between different actions such as search and rescue, evacuation, inspection, building stabilization and repair, retrieval of possessions, or re-occupation in an aftershock-prone zone. This issue can be further complicated by progressive deterioration in the structures, induced by an ongoing sequence of aftershock events. An operational aftershock damage forecasting framework can provide a quantified support basis for rapid decision-making. Such a framework can be built based on analytic predictions of structural performance as a function of the time elapsed after the main earthquake event. The mean daily rate of exceeding a prescribed limit state can be regarded as an operational and probability-based proxy for time-dependent structural performance. This work focuses on the issues that can arise in time-dependent performance-based fragility assessment in the presence of an ongoing aftershock sequence.

Recently, many studies have been conducted in order to address the time-dependent issues related to seismic aftershock risk assessment. Li and Ellingwood [1] proposed a probabilistic approach for post-earthquake performance assessment of steel frame buildings. In the absence of ground motion records to describe the main shock-aftershocks sequence, it was assumed that the aftershocks are modeled by ensembles of the main-shock ground motions to be appropriately scaled using relations established between the main-shock and aftershock intensities. They concluded that the characteristics of the aftershocks have a significant influence on the structural damage pattern. Yeo and Cornell [2] have proposed a decision-making framework based on stochastic dynamic programming which minimizes the expected life-cycle cost subjected to acceptable life-safety constraints. As a proxy for life-safety, they have employed an equivalent constant collapse rate for the main-shock damaged structure (Yeo and Cornell [3]). Goda and Taylor [4] studied the peak ductility demand for inelastic single degree of freedom (SDOF) systems using both real and artificially generated main shock-aftershock sequences based on seismological models. They showed that by using the real sequences, the incremental effects of aftershocks on the peak ductility demand were relatively small. Meanwhile, using artificially-generated sequences, the additional aftershock effects on the peak ductility demand were found to be significant.

Jalayer et al. [5] proposed a probabilistic methodology, based on successive applications of the Total Probability theorem [6], for calculating the rate of exceeding a prescribed *limit state* (*LS*) in the time elapsed after the occurrence of the main event. In this approach, the time-variant daily rate of exceeding the *collapse* limit state is adopted as a proxy for life-safety considerations. In this study, the main-shock-after-shock sequence was approximated by a sequence of strong-motion events. The present study is based on a modified version of the methodology presented in [5] which is adapted to an operation forecasting framework. A non-linear time-dependent performance variable, defined as the ratio of maximum demand increment to residual capacity, is adopted herein to represent the evolution in structural performance. Daily fragility curves, expressed as the conditional probability that the performance variable exceeds unity in a 24 hour interval (given seismic intensity), are used to represent the time-dependent vulnerability of the structure. The daily fragility curves are calculated as a sum of a sequence of *event-based* fragility curves that are weighted by the probability that a certain number of aftershock events take place in the considered interval. The event-based fragilities are calculated by linear logarithmic regression of the structural performance variable versus seismic intensity (represented by the first-mode spectral acceleration) subjected to a series of plausible seismic sequences in order to model the record-to-record uncertainty in structural response assessment. This method is referred to herein as the *sequential cloud analysis* since it is inspired from a non-linear dynamic structural analysis procedure known as the

cloud method [7].The set of seismic sequences are selected through alternative approaches, namely, (a) permutation of real aftershock events taken from the ongoing sequence; (b) ”cloning“ of real aftershock events (repeating the same wave-form for a number of times); (c) permutation of a set of strong-motion wave-forms scaled so that their median is equal to the median spectral acceleration of the real aftershocks (i.e., the so-called *cloud scaling*, described later); (d) cloning of a set of strong-motion wave-forms ”clone-scaled“ to the median spectral acceleration of the real aftershocks. The probability that a certain number of aftershock events of interest take place in a 24 hour time interval is calculated from two alternative aftershock occurrence models. These occurrence models are based on, (a) an epidemiologic space-time point process model known as ETAS [8, 9]; (b) the modified Omori model assuming a non-homogenous Poisson occurrence [10]. The mean daily rate of exceeding a given limit state is calculated next by integrating the daily rate of exceeding a given spectral acceleration (probabilistic aftershock hazard analysis, PASHA, see [11]) and the daily fragility curve for the limit state in question.

As a numerical example, daily forecasts of the mean rate of exceeding two ultimate *LS*'s are performed for the L'Aquila aftershock sequence (2009, central Italy). As the structural model, an equivalent SDOF model with cyclic strength and stiffness deterioration is used in order to study the damage induced as a result of the sequence of aftershocks. The first excursion points for both *LS*'s due to the L'Aquila sequence are also used as a benchmark for the calculations.

1.1 Definition of daily forecasting

In an operational forecasting framework, daily fragility curves for a given limit state can be predicted for a time interval (usually equal to or less than 24 hour) defined as $[T_{start}, T_{end}]$ for the *j*th day, $j = 1, \ldots, N_{\text{day}}$ (where N_{day} denotes the number of days of interest for decision-making purposes). The sequence aftershock wave-forms (registered in a temporary catalog) in the time elapsed between the main-shock until T_{start} is denoted as $\mathbf{seq}$. However, the aftershock events occurring in the *forecasting interval* $[T_{start}, T_{end}]$ need to be generated (as will be discussed hereafter). These generated sequences are denoted by $\mathbf{seq}_{\text{gen}}$.

2 TIME-DEPENDENT VULNERABILITY ASSESSMENT

2.1 Structural performance variable *Y*

Residual drift demands are recognized as key response parameters in the short- and long-term performance-assessment of existing buildings [12-14]. Let N_{as} be the number of aftershock events taking place in the forecasting interval $[T_{start}, T_{end}]$ associated with *j*th day after the main event. Each event n, $n = 1, \ldots, N_{\text{as}}$, may lead to an increase in the peak and residual drift demands in the damaged structure, based on its amplitude and frequency content as well as the hysteretic characteristics of the structure (see [15, 16]). Arguably, the structural response to the *n*th event is significantly affected by the residual (permanent) drift demand due to (*n*-1) previous events.

In this work, a novel scalar time-dependent performance variable, suitable for sequential evaluation of demand and capacity in the structure, is introduced as the ratio of maximum demand increment due to the sequence of *n* events and the residual drift capacity in the structure:

$$Y_{LS}^{(n)} = \frac{D_{\max}^{(n)} - D_{\mathrm{r}}^{(n-1)}}{C_{LS} - D_{\mathrm{r}}^{(n-1)}} \tag{1}$$

where $D_{\max}^{(n)}$ is the maximum drift demand due to the sequence of *n* events, $D_r^{(n-1)}$ is the residual drift demand corresponding to the sequence of (*n*-1) events, and C_{LS} is the capacity of the (intact) structure for the desired limit state. The term $D_{\max}^{(n)} - D_r^{(n-1)}$ can be interpreted as the maximum increment in the story drift due to the *n*th event; meanwhile, the term $C_{LS} - D_r^{(n-1)}$ can be viewed as the structural residual drift capacity right after the sequence of (*n*-1) events. Note that at the onset of *LS*, the maximum drift demand is equal to the *LS* capacity (i.e., $D_{\max}^{(n)} = C_{LS}$). Hence, the performance variable Y_{LS} is equal to unity at the onset of the *LS*. It is interesting to note that the performance variable in Equation (1), which derived for maximum inter-story drift, can be generalized (see [17]) in order to take into account a range of potential failure mechanisms (*cut-sets*):

$$Y_{LS}^{(n)} = \max_{l=1}^{N_{\mathrm{mech}}} \min_{m=1}^{N_l} Y_{m,l}^{(n)} \tag{2}$$

where N_{mech} is the number of potential failure mechanisms; N_l is the number of components in the *l*th mechanism; and $Y_{m,l}^{(n)}$ is the structural performance index for the *m*th component of the *l*th mechanism, defined in Equation (1). This generalized performance variable can be interpreted as the component demand to capacity ratio that brings the system closer to the first *LS* excursion (see [17] for more detail). This generalized formulation can be quite useful for shear-critical structures.

2.2 A probabilistic performance-based framework for aftershock forecasting

A probabilistic performance objective for aftershock forecasting can be achieved by ensuring that the daily rate of exceeding a prescribed limit state denoted by λ_{LS} is smaller than or equal to an admissible rate denoted by λ_{admis}:

$$\lambda_{LS} = \lambda\left(Y_{LS} \geq 1\right) \leq \lambda_{\mathrm{admis}} \tag{3}$$

where the mean daily rate of exceeding a limit state is equal to the mean daily rate that the performance variable Y_{LS} corresponding to *LS* is greater than or equal to unity. In order to take into account only the aftershock events of interest, the daily limit state rate λ_{LS} can be written as:

$$\lambda_{LS} = \lambda\left(Y_{LS} \geq 1\right) = \lambda\left(M \geq M_l\right) \cdot P\left(Y_{LS} \geq 1 \,|\, M \geq M_l\right) \tag{4}$$

where $\lambda\left(M \geq M_l\right)$ is the time-dependent daily rate of occurrence of aftershocks with magnitude larger than or equal a cut-off magnitude M_l and $P\left(Y_{LS} \geq 1 \,|\, M \geq M_l\right)$ is the probability of exceeding the limit state *LS* given $M \geq M_l$, referred to as the seismic aftershock risk hereafter.

2.3 Time-dependent risk assessment

let $\mathbf{I}_j$ denote the following information[1]: A **seq** of aftershock events with $M \geq M_l$ in the forecasting interval $[T_{start}, T_{end}]$ corresponding to the *j*th day. The probability of exceeding a specified *LS* can be expanded as follows (using the Total Probability Theorem):

$$P\left(Y_{LS} \geq 1 | \mathbf{I}_j\right) = \sum_{n=1}^{N_{as}} P\left(Y_{LS} \geq 1 | n, \mathbf{I}_j\right) P\left(n | \mathbf{I}_j\right) \tag{5}$$

where N_{as} denotes the maximum number of aftershock events in the forecasting interval; $P\left(Y_{LS} \geq 1 | n, \mathbf{I}_j\right)$ is the probability of exceeding the *LS* given that exactly n aftershock events take place; and $P\left(n | \mathbf{I}_j\right)$ is the probability that exactly n events take place in the prescribed time interval. The term $P\left(LS | n, \mathbf{I}_j\right)$ can be further decomposed[2] by introducing the spectral acceleration *x* as an interface variable:

$$P\left(Y_{LS} \geq 1 | n, \mathbf{I}_j\right) = \int_x P\left(Y_{LS} \geq 1 | x, n, \mathbf{I}_j\right) \left| \mathrm{d}P\left(S_a(T) > x | n, \mathbf{I}_j\right) \right| \tag{6}$$

where $P\left(Y_{LS} \geq 1 | x, n, \mathbf{I}_j\right)$ is the structural *fragility* defined as a function of the spectral acceleration at the specified period $S_a(T) = x$; $P\left(S_a(T) > x | n, \mathbf{I}_j\right)$ is the probability that an aftershock event has a spectral acceleration greater than *x*[3]. It is interesting to note that

$$\mathrm{d}\lambda\left(x | \mathbf{I}_j\right) = \lambda\left(M \geq M_l | \mathbf{I}_j\right) \cdot \mathrm{d}P\left(S_a(T) > x | \mathbf{I}_j\right) \tag{7}$$

where $\lambda\left(M \geq M_l | \mathbf{I}_j\right)$ is the time-dependent daily rate of occurrence of aftershocks with $M \geq M_l$ and $\lambda\left(x | \mathbf{I}_j\right)$ is the mean daily rate of exceedance of a given level of $S_a(T)$ equal to x (also referred to as daily forecasting of aftershock hazard, [11]).

2.3.1 *Estimating the number of events P(n|I_j)*

As mentioned in the introduction, this work employs two well-established earthquake occurrence models suitable for daily seismicity forecasts associated with the evolution of an aftershock sequence; the Modified Omori's aftershock model (MO) [10] with updated parameters based on the aftershocks that have already occurred, i.e. the **seq**, (see [5, 11]) and the Epidemic Type Aftershock Sequence (ETAS) model [8, 9, 18]. The daily seismic aftershock hazard $\lambda\left(x | \mathbf{I}_j\right)$ can be calculated based on both occurrence models [11]. Accordingly, the probability $P\left(n | \mathbf{I}_j\right)$ that exactly *n* events take place in the forecasting interval on *j*th day (i.e. Equation 5) can be estimated based on both MO and ETAS occurrence models.

[1] This is done for simplifying the formulation and will be used to remind that the risk calculations are conditioned on background information $\boldsymbol{I_j}$. Needless to say, also $\boldsymbol{I_j}$ represents a time-dependent set of information.
[2] Using the Total Probability Theorem
[3] It is assumed that knowing the exact number of aftershock events *n* with magnitude greater than or equal to a lower cut-off level is not going to affect the aftershock hazard. Therefore the dependence on *n* is dropped hereafter. This assumption may be justified by the fact that the forecasted hazard for the *j*th day is does not take into account the events occurring within the forecasting time window (see [11]).

ETAS: ETAS model accounts for the triggering effect of all the events that have occurred before T_{start} and those that will occur during the forecasting interval $\left[T_{start}, T_{end}\right]$. Since the latter are unknown at the moment of the forecast, they can be simulated. For instance, Marzocchi and Lombardi [9] have simulated N=500 different synthetic daily catalogs by using the "thinning method" proposed by Ogata [18]. Based on the N simulated catalogs and the **seq**, the N different realizations of the number of events N_{as} (occur in the forecasting interval) can be obtained based on ETAS model [11]. Therefore, $P\left(n \mid \mathbf{I}_j\right)$ can be estimated with an empirical probability distribution for the various realizations of N_{as}.

Modified Omori (MO): $P\left(n \mid \mathbf{I}_j\right)$ can also be estimated by a non-homogenous Poisson probability distribution with the time-decaying rate based on the MO model:

$$P\left(n \mid \mathbf{I}_j\right) = \frac{\lambda_{\text{MO}}\left(M \geq M_l \mid \mathbf{I}_j\right)^n e^{-\lambda_{\text{MO}}\left(M \geq M_l \mid \mathbf{I}_j\right)}}{n!} \tag{8}$$

where $\lambda_{\text{MO}}\left(M \geq M_l \mid \mathbf{I}_j\right)$ is the daily rate of having aftershock events with $M \geq M_l$ based on the MO occurrence model (for more details see [5, 11]).

2.3.2 *Time-dependent vulnerability assessment*

The fragility term $P\left(Y_{LS} \geq 1 \mid x, n, \mathbf{I}_j\right)$ in Equation (6) can be calculated by taking into account the set of mutually exclusive and collectively exhaustive (MECE) events that the *LS* is exceeded at one and just one of the previous aftershock events (first excursion, see also [19]):

$$P\left(Y_{LS} \geq 1 \mid x, n, \mathbf{I}_j\right) = P\left(C_1 + \overline{C_1}C_2 + \overline{C_1}\,\overline{C_2}C_3 + \ldots + \overline{C_1}\,\overline{C_2}\ldots\overline{C_{n-1}}C_n \mid x, n, \mathbf{I}_j\right) \tag{9}$$

where $C_k, k = 1{:}n$ is defined as:

$$\begin{cases} C_k \equiv Y_{LS} \geq 1 \text{ after } k\text{th event} \\ \overline{C}_k \equiv Y_{LS} < 1 \text{ after } k\text{th event (read as not } C_k) \end{cases} \tag{10}$$

Since the events $\overline{C_1 C_2 \ldots C_{k-1}}C_k, k = 1{:}n$ are MECE, Equation (9) can be re-written by summing up the probabilities for each separate term[4]:

$$P\left(Y_{LS} \geq 1 \mid x, n, \mathbf{I}_j\right) = \sum_{k=1}^{n} P\left(\overline{C_1 C_2 \ldots C_{k-1}}C_k \mid x, \mathbf{I}_j\right) \tag{11}$$

where $P\left(\overline{C_1 C_2 \ldots C_{k-1}}C_k \mid x, \mathbf{I}_j\right)$ represents the sequence of fragility terms identified by the fact that the first *LS* excursion takes place at *k*th event This fragility term can be expanded as[5]:

[4] Note that the dependence on *n* is dropped for simplicity. In any case, the fact that *n* events have taken place is already reflected in the summation.

[5] In the previous articles by the authors [5] and [20], it was assumed that the C_k's are stochastically independent. Therefore, the formulation presented in Equation (12) is general and is obtained based on the *product rule* in probability [21].

$$P\left(\overline{C_1C_2....C_{k-1}}C_k \mid x,\mathbf{I}_j\right)=P\left(C_k \mid \overline{C_1C_2....C_{k-1}},x,\mathbf{I}_j\right)P\left(\overline{C_1C_2....C_{k-1}} \mid x,\mathbf{I}_j\right) \quad (12)$$

where $P\left(C_k \mid \overline{C_1C_2....C_{k-1}},x,\mathbf{I}_j\right)$ denotes the structural fragility when the first *LS* excursion takes place after the occurrence of the *k*th event, and $P\left(\overline{C_1C_2....C_{k-1}} \mid x,\mathbf{I}_j\right)$ is the probability that the structure has not exceeded the limit state after the (*k*-1)th event. The latter can be further expanded as (by following the same logics as in Equations 10 and 12):

$$P\left(\overline{C_1C_2....C_{k-1}} \mid x,\mathbf{I}_j\right)=\left[1-P\left(C_{k-1} \mid \overline{C_1C_2....C_{k-2}},x,\mathbf{I}_j\right)\right]P\left(\overline{C_1C_2....C_{k-2}} \mid x,\mathbf{I}_j\right) \quad (13)$$

In a recursive manner, one can obtain the following expression:

$$P\left(\overline{C_1C_2....C_{k-1}} \mid x,\mathbf{I}_j\right)=\prod_{i=1}^{k-1}\left[1-P\left(C_i \mid \overline{C_1C_2....C_{i-1}},x,\mathbf{I}_j\right)\right] \quad (14)$$

Thus, substituting $P\left(\overline{C_1C_2....C_{k-1}} \mid x,\mathbf{I}_j\right)$ from Equation (14) in Equation (12):

$$P\left(\overline{C_1C_2....C_{k-1}}C_k \mid x,\mathbf{I}_j\right)=P\left(C_k \mid \overline{C_1C_2....C_{k-1}},x,\mathbf{I}_j\right)\prod_{i=1}^{k-1}\left[1-P\left(C_i \mid \overline{C_1C_2....C_{i-1}},x,\mathbf{I}_j\right)\right] \quad (15)$$

Finally, substituting $P\left(\overline{C_1C_2....C_{k-1}}C_k \mid x,\mathbf{I}_j\right)$ from Equation (15) in Equation (11), one can calculate the *event-dependent* fragility $P\left(Y_{LS}\geq 1 \mid x,n,\mathbf{I}_j\right)$:

$$P\left(Y_{LS}\geq 1 \mid x,n,\mathbf{I}_j\right)=\sum_{k=1}^{n}\left(P\left(C_k \mid \overline{C_1C_2....C_{k-1}},x,\mathbf{I}_j\right)\cdot\prod_{i=1}^{k-1}\left[1-P\left(C_i \mid \overline{C_1C_2....C_{i-1}},x,\mathbf{I}_j\right)\right]\right) \quad (16)$$

The *event-dependent* fragility term $P\left(Y_{LS}\geq 1 \mid x,n,\mathbf{I}_j\right)$ is estimated herein by a novel nonlinear dynamic analysis procedure presented herein as the *sequential cloud analysis* procedure.

3 SEQUENTIAL CLOUD ANALYSIS

The sequential cloud analysis procedure outlined in this section leads to the calculation of the sequence of fragility terms $P\left(\overline{C_1C_2....C_{k-1}}C_k \mid x,\mathbf{I}_j\right)$, $k\in\langle 1,\ldots,n\rangle$ in Equation (11).

Let N_{seq} be the number of wave-form sequences $\mathbf{seq}_{\text{gen}}$ generated to model the sequence of aftershocks taking place in the forecasting interval. In the operational forecasting context, this means that the generated sequences $\mathbf{seq}_{\text{gen}}$ are going to be applied to the structure that has been already subjected to the sequence of events preceding the forecasting window denoted as **seq** beforehand (i.e., structural state at T_{start}). Each sequence $\mathbf{seq}_{\text{gen}}$ consists of N_{as} waveforms that generically substitutes/represents the number of events *k*. While the structure is subjected to N_{seq} suites of sequences $\mathbf{seq}_{\text{gen}}$, for each aftershock event *k*, a set of N_{seq} structural performance variables $Y_{LS}^{(k,m)}$, $m\in\langle 1,\ldots,N_{\text{seq}}\rangle$ can be calculated.

The performance variable $Y_{LS}^{(k,m)}$ is calculated by subjecting the structure (damage state at T_{start}) to the *m*th sequence of *k* events in the suite of N_{seq} sequences generated. The spectral acceleration value corresponding to $Y_{LS}^{(k,m)}$ and denoted by $S_a^{(k,m)}$ is defined as the elastic

small-amplitude[6] spectral acceleration of the last (*k*th) aftershock event in the *m*th sequence of events. However, in order to create the condition $\overline{C_1 C_2 ....C_{k-1}} C_k$, those $Y_{LS}^{(k,m)}$ values for which the structure has already exceeded the *LS* threshold in the previous $(k-1)$ steps are not taken into account. This entails a sample reduction and the effective cloud sample size may be reduced from N_{seq} to $N_{\text{seq}}^{\text{red}}(k)$. In short, the cloud analysis, given *k* aftershock events, leads to a suite of $Y_{LS}^{(k,m)}$ values, $m \in \langle 1, \ldots, N_{\text{seq}}^{\text{red}}(k) \rangle$.

Assuming that the (conditional) distribution of critical demand-to-capacity ratio Y_{LS} for a given level of $S_a(T) = x$ is described by a lognormal distribution, the *k*th fragility term $P\left(C_k \mid \overline{C_1 C_2 ....C_{k-1}}, x, \mathbf{I}_j\right)$ in Equation (16), can be expressed as:

$$P\left(C_k \mid \overline{C_1 C_2 ....C_{k-1}}, x, \mathbf{I}_j\right) = P\left(Y_{LS}^{(k)} \geq 1 \mid x, \mathbf{I}_j\right) = 1 - \Phi\left(\frac{-\ln \eta_{Y|Sa}^{(k)}(x)}{\beta_{Y|Sa}^{(k)}}\right) \tag{17}$$

where (see [22]):

$$\ln \eta_{Y|Sa}^{(k)}(x) = a + b \ln(x)$$
$$\beta_{Y|Sa}^{(k)} = \sqrt{\frac{\sum_{m=1}^{N_{\text{cloud}}^{\text{red}}(k)} \left[\ln\left(\frac{Y_{LS}^{(k,m)}}{a \cdot \left(S_a^{(k,m)}\right)^b}\right)\right]^2}{N_{\text{cloud}}^{\text{red}}(k) - 2}} \tag{18}$$

where $N_{\text{cloud}}^{\text{red}}(k)$ is the effective cloud sample size given *k* aftershock events; *a* and *b* are the coefficients of the logarithmic linear regression (see [5, 22] for more details). $\eta_{Y|Sa}^{(k)}$ and $\beta_{Y|Sa}^{(k)} = \sigma_{\ln Y|Sa}^{(k)}$ are the conditional median and the conditional standard deviation of the natural logarithm of $Y_{LS}^{(k)}$ given spectral acceleration and that *k* aftershock events have occurred; $Y_{LS}^{(k)}$ is the structural performance variable given a sequence of *k* aftershock events.

4 NUMERICAL EXAMPLE

The methodology described in Sections 2 and 3 is applied in order to perform an adaptive performance-based aftershock risk assessment for an SDOF system, representative of an existing RC building.

4.1 The L'Aquila aftershock sequence

On April 6, 2009, at 1:32 AM UTC (i.e., Universal Time Coordinated), an earthquake with local magnitude (Ml) equal to 5.9 struck central Italy in the Abruzzo region underneath the town of L'Aquila which is located approximately 6 km from the epicenter. The large shock triggered a vigorous aftershock sequence, which spread within the first twenty-four hours over

[6] It is noteworthy that using the spectral acceleration at the secant period of the damaged structure due to the deteriorating effects of previous events (i.e. those within the **seq**) might provide a better correlation with the performance variable. However, it has been decided herein to use the elastic small-amplitude period spectral acceleration as the seismic intensity measure.

a secondary seismogenetic structure north of L'Aquila. The reference structure's hypothetic site is located near the recording station "L'Aquila - V. Aterno - Aquil Park Ing" (AQK), ITDPC network (Italian ACcelerometric Archive, ITACA, http://itaca.mi.ingv.it/ItacaNet/).

In order to generate operative daily earthquake occurrence forecasts based on ETAS and MO models (which are directly implemented in the probabilistic aftershock hazard analysis, PASHA), a provisional and quasi real-time catalog used by Marzocchi and Lombardi [9] is utilized by the authors (see also [11]). This is to reflect the fact that immediately after a main-shock, one often needs to make reference to a provisional catalog. In addition to the catalog, the waveform archive of L'Aquila aftershock sequence registered between 30 March 2009 and 30 April 2009 is used. This archive consists of recordings by DPC-RAN (Rete Accelerometrica Nazionale) (35 stations) and by INGV (Istituto Nazionale di Geofisicae Vulcanologia) (29 stations) permanent and temporary seismic networks. The database of wave-forms is one of the products related to the Project S5 "High-resolution multi-disciplinary monitoring of active fault test-site areas in Italy" in Task 4 UR6 WP 4.3 (http://dpc-s5.rm.ingv.it/en/S5.html). Consequently, the waveforms corresponding to each aftershock events listed within the catalog are post-processed and extracted from long-format time-windows [11].

The sequence of aftershock events **seq** consists of the aftershock wave-forms registered in the above-mentioned catalog after the main-shock up to 6:00 AM UTC of the upcoming day (i.e. *j*th day). The sequence **seq** is used to: (a) estimate the time-decaying parameters of the MO model [11]; (b) estimate the time dependent rate $\lambda\left(M \geq M_l \,|\, \mathbf{I}_j\right)$ based on both ETAS and MO models, as shown in the subsequent section (see also [11]); (c) perform time-dependent PASHA; (d) obtain the distribution $P\left(n \,|\, \mathbf{I}_j\right)$ based on both ETAS and MO models; and (e) construct the suite of ground motion sequences $\mathbf{seq}_{\text{gen}}$.

4.1.1 *The estimated number of events*

The number of registered aftershock events per day with magnitude greater than or equal to 3.3 is illustrated in Figure 1 in the time period from April 6, 2009, at 6:00 UTC, (i.e., a few hours after the main event) up to May 10, 2009. The forecasted of number of events with $M \geq 3.3$ per day based on both MO and ETAS models are also shown in the figure. It can be depicted from Figure 1 that both models perform quite well in capturing the trend in the number of aftershocks. Moreover, it can be observed that the ETAS tends to provide an upper-bound estimate of the number of events.

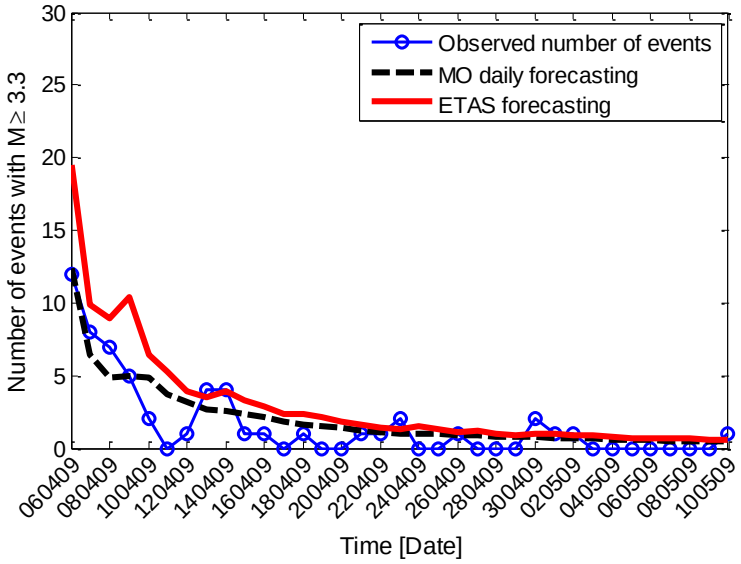

Figure 1: The observed and forecasted number of events ($M \geq 3.3$) per day.

4.2 The limit states

The performance objectives for post-earthquake assessment of the case-study structure are defined in terms of discrete *LS*'s of *Serviceability*, *Damage Limitation* (DL), *Significant Damage* (SD) and *Near Collapse* (NC). The last three *LS*'s are based on the European standard EC8-3 [23]. The *LS*'s are distinguished herein in terms of increasing levels of the maximum displacement for the equivalent SDOF system. In this study, it has been assumed that the ultimate displacement corresponding to a 20% drop in strength is representative of the NC limit state. Table 1 outlines the maximum displacements for the equivalent SDOF system identifying these *LS*'s.

LS	Maximum Displacement (meters)
Serviceability	0.01
Damage Limitation (DL)	0.02
Significant Damage (SD)	0.05
Near Collapse (NC)	0.07

Table 1: *LS*'s threshold for the equivalent SDOF

4.3 The structural model

An equivalent degrading (SDOF) system is utilized as the structural model. The case-study system is a modified version of the SDOF model which has been extensively used by the authors in previous works (see [5, 20, and 24]). The reference building is a generic five-story RC frame structure designed to resist seismic actions. The equivalent SDOF system has period $T = 0.58\text{sec}$, damping $\zeta = 5\%$, yield displacement $D_y = 0.02$ (meters), ultimate displacement $D_u = 0.15$ (meters), strength reduction factor $R = 2$, ductility $\mu = 2.5$, post yield stiffness ratio $\alpha_h = 0.17$, and no residual deformations. Based on the resulting equivalent pushover (capacity) curve, a non-linear degrading hysteresis model for the equivalent SDOF system is constructed. Figure 2a demonstrates the capacity curve for the equivalent SDOF

system where the onset of various limit states is marked. The figure also shows the maximum and residual displacement demand induced due to L'Aquila 2009 main event. It can be observed that the structure has exceeded the state of DL while it falls below the SD limit state. Moreover, the residual displacement of the system has exceeded the Serviceability limit state and it is just a little lower than the state of DL. This equivalent SDOF system seems to represent the category of structures that can be quite vulnerable to the aftershocks. In other words, although the structure has not experienced very high level of damages due to the main-shock, it has the growing potential of moving toward higher damage levels under the sequentially-applied aftershock events.

The sequential time history analyses are performed with the Open System for Earthquake Engineering Simulation (OPENSEES, http://opensees.berkeley.edu) by employing a hysteresis model with pinching that exhibits cyclic degradation in unloading and reloading stiffness as well as strength degradation (Pinching4 Material). Figure 2b represents the hysteresis behavior of the structure in response to a periodic loading protocol.

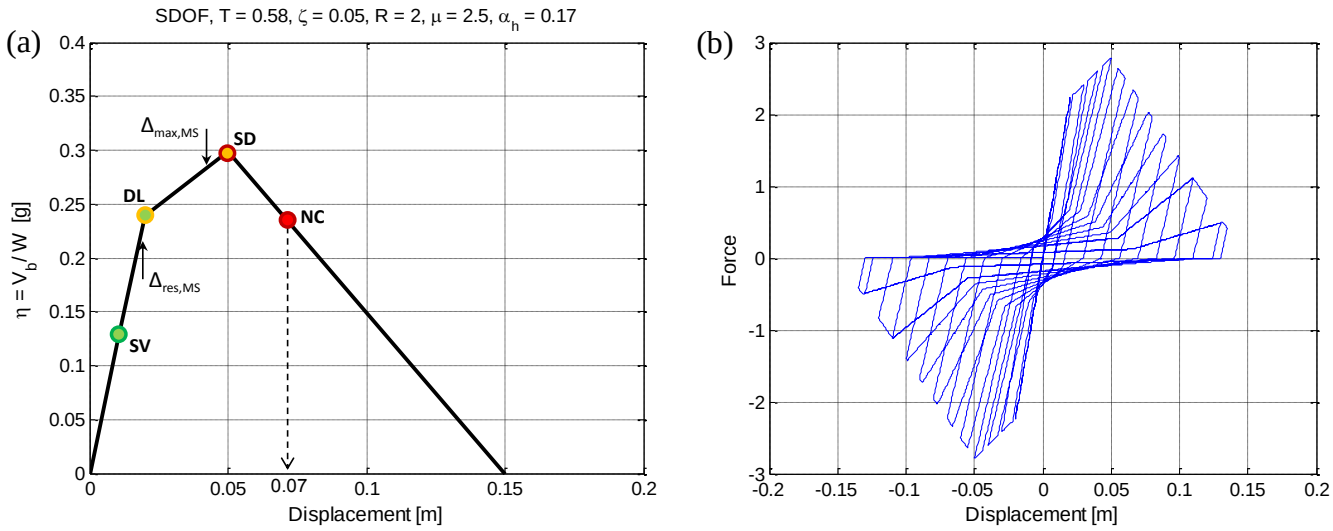

Figure 2: Equivalent SDOF system (a) the capacity curve, (b) the hysteresis behavior

4.4 Estimating number of aftershocks per day

As mentioned before, the probability distribution for the number of events $P\left(n \mid \mathbf{I}_j\right)$ can be estimated based on both MO and ETAS occurrence models (see Section 2.3.1). Figure 3 illustrates the histogram for the number of ETAS forecasted events with $M \geq 3.3$ [9] for date 06/04/09. This histogram can also be used in order to estimate the number of aftershocks N_{as} that are expected to happen per day. For example, a best-estimate of N_{as} for the forecasting interval of 06/04/09 can be calculated as $\left(\text{mean} + \sqrt{3}\,\text{sigma}\right)$ for the distribution $P\left(n \mid \mathbf{I}_j\right)$ based on ETAS model (as shown in Figure 3). Accordingly, $P\left(n \mid \mathbf{I}_j\right)$, $n = 1, \ldots, N_{\text{as}}$ are shown in Figure 4 for the first 4 days elapsed after the main event, namely, from 06/04/09 up to date 09/04/09. Equation (8) is used to estimate the probability distribution for the number of events based on a non-homogenous Poisson distribution (MO).

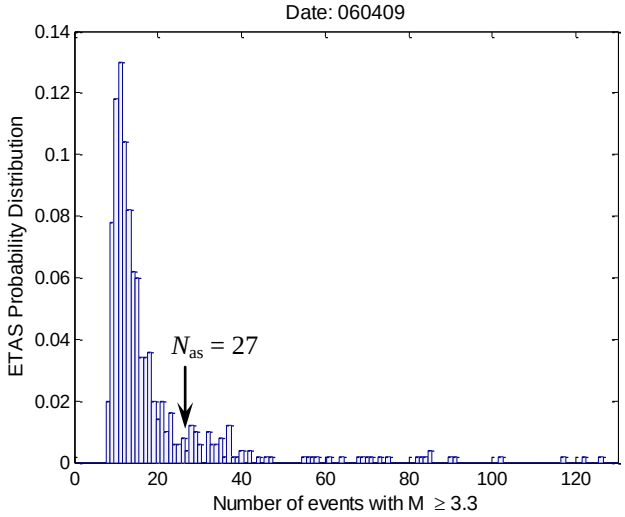

Figure 3: The histogram of the ETAS forecasted number of events for the day 06/04/09. N_{as} is a best-estimate for the number of events based on ETAS model

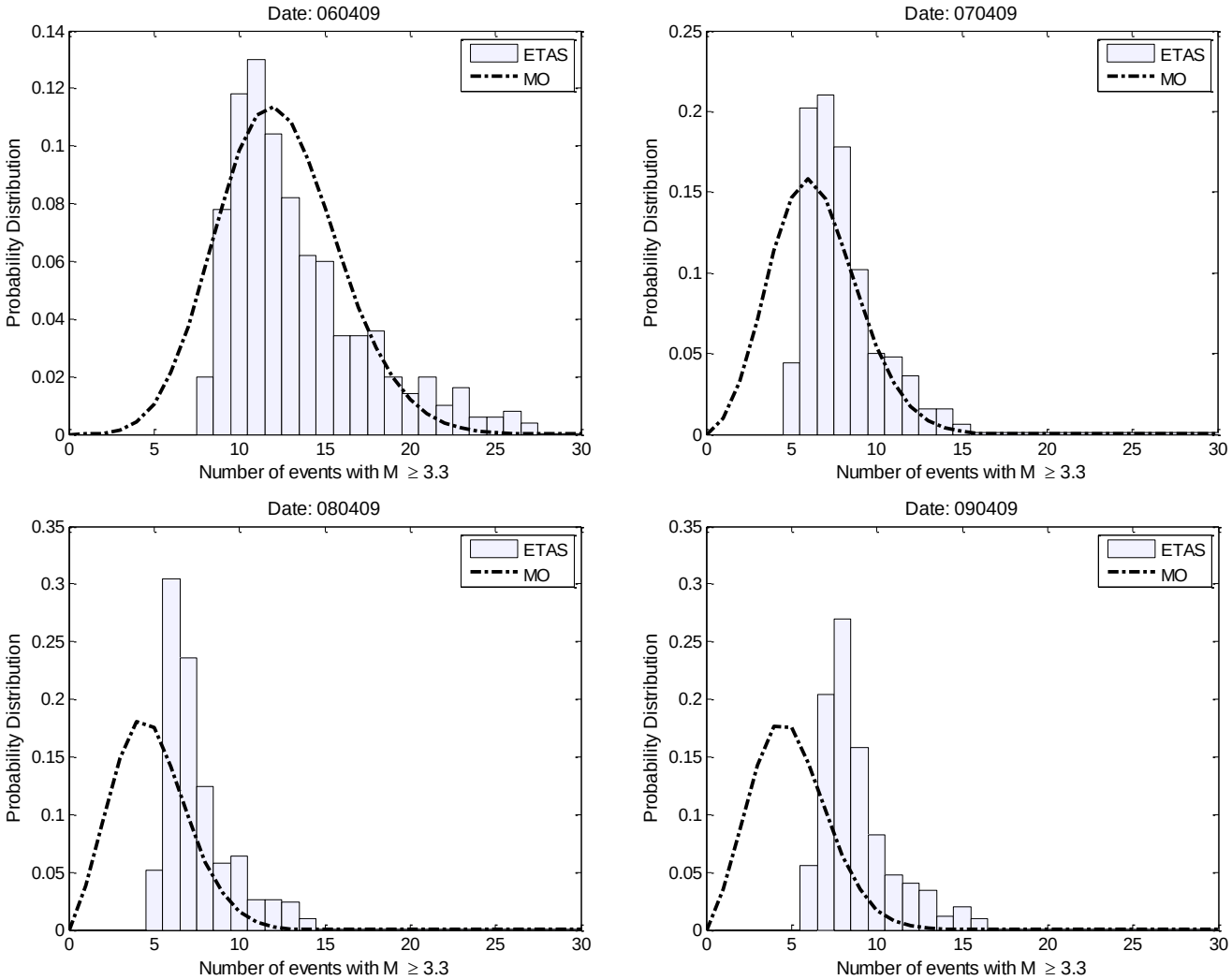

Figure 4: The distribution of the number of events per day based on MO and ETAS models

It can be observed that the ETAS predictions for the number of events are systematically larger than those of non-homogenous Poisson distribution based on MO model. Moreover, it can be seen that the MO Poisson model assigns a non-zero probability to having very few aftershock events (i.e., in the order of 5-10). On the contrary, ETAS assigns zeros probability to the possibility of having very few aftershock events. This is expected to affect the daily fragility curves which are going to be calculated as a weighted sum, equal to $P\left(n \mid \mathbf{I}_j\right)$, of event-dependent fragilities.

4.5 The selection of the suite of aftershock sequences

In the sequential cloud analysis, the selection of the suites of the aftershock records denoted as $\mathbf{seq}_{\text{gen}}$ is expected to play an important role. Previous studies on the effect of seismic sequences on the response of structures typically employed artificial sequences using the main-shock wave-form as a seed for simulating the aftershocks based on two different schemes: the so-called *back-to back* approach, and randomization (see [13] for an extensive review of these approaches). It is also interesting to study the possibility of employing recorded ground motions. The archive of L'Aquila sequence waveforms within the first month after the main event provides an opportunity to study the issues related to ground motion record selection for the non-linear dynamic analysis procedures such as the sequential cloud. In this work 4 different ground motion selections strategies, relying in real ground motion recordings, are studied:

a. Generate N_{seq} suites of ground motion sequences $\mathbf{seq}_{\text{gen}}$ of N_{as} records by random permutation (with replacement) of the wave-forms recorded in the available sequence $\mathbf{seq}$. As mentioned before, the sequence $\mathbf{seq}$ consists of records registered before the forecasting interval $\left[T_{start}, T_{end}\right]$.
b. Generate N_{seq} suites of ground motion sequences $\mathbf{seq}_{\text{gen}}$ of N_{as} records by repeating N_{as} times (also referred to as *cloning*) the various wave-forms recorded in the available sequence $\mathbf{seq}$. As the sequence evolves, there are more records available to select.
c. Generate N_{seq} suites of ground motion sequences $\mathbf{seq}_{\text{gen}}$ of N_{as} records by random permutation (with replacement) of a selection of strong-motion wave-forms that are scaled so that their median spectral acceleration $S_a(T)$ is equal to the median of the spectral acceleration values for the aftershock records registered within $\mathbf{seq}$.This is referred to hereafter as the *cloud-scaling*.
d. Generate N_{seq} suites of ground motion sequences $\mathbf{seq}_{\text{gen}}$ of N_{as} records by repeated cloning of a selection of strong-motion wave-forms that are cloud-scaled to the median $S_a(T)$ of the aftershocks within $\mathbf{seq}$.

The outcome of the sequential cloud method depends clearly on the choice of the parameters N_{as} and N_{seq}. For record selection based on the wave-forms within $\mathbf{seq}$, more and more records become available as days pass. Therefore, N_{seq} can be increased in order to increase the precision of the cloud method. On the other hand, the expected number of aftershock per

day is going to decrease with time. Table 2 outlines the values adopted for N_{as} and N_{seq} in the first four days elapsed after the main event.

Target Date	Best estimate for the number of events, N_{as}	Number of events within the **seq**, N_{seq}
06/04/09	27	15
07/04/09	15	22
08/04/09	14	29
09/04/09	16	38

Table 2: N_{as} and N_{seq} values for the first 4 days after the main-shock

4.6 The daily fragility curves

It is described herein how the daily fragility curves for the limit state of SD for the second day (j=2) elapsed after the main event can be calculated[7]. As it can be observed from Table 2, $N_{\text{as}} = 15$ and $N_{\text{seq}} = 22$. The step-by-step approach for fragility assessment is outlines below:

1. The sequence of fragility curves $P\left(C_k \mid \overline{C_1 C_2 .... C_{k-1}}, x, \mathbf{I}_2\right)$, $k \in \langle 1, \ldots, n \rangle$ is first calculated from Eq. (17) by employing the sequential cloud analysis described in Section 3. Figure 5 illustrates the sequence of N_{as} fragility curves calculated for the second day based on record selection strategy (a) (described in the previous section).
2. The sequence of event-dependent fragility curves $P\left(Y_{LS} \geq 1 \mid x, n, \mathbf{I}_2\right)$, $n \in \langle 1, \ldots, N_{\text{as}} \rangle$ are calculated next from Eq. (16), based on the fragility sequence calculated in the previous step. Figure 6 shows the sequence of fragility curves $P\left(Y_{LS} \geq 1 \mid x, n, \mathbf{I}_2\right)$.
3. The fragility curve for the second day $P\left(Y_{LS} \geq 1 \mid x, \mathbf{I}_j\right)$ can be finally calculated from Equations (5) and (6) as a weighted sum of $P\left(n \mid \mathbf{I}_2\right)$ (see Figure 4) and $P\left(Y_{LS} \geq 1 \mid x, n, \mathbf{I}_2\right)$. Figure 6 also demonstrates forecasted fragility curve for the second day based on both ETAS and MO models. Note that the difference between the forecasted fragility curves can be attributed to the difference between their associated probability distributions $P\left(n \mid \mathbf{I}_2\right)$, as shown in Figure 4.

As a benchmark for the forecasted fragility curves, the first-excursion point for the SD is marked with probability 1 on Figure 6. For the previous events, a point with probability zero is shown on the figure. Note that this benchmark points are created by means of *hind-sight*[8] based on the records registered in the forecasting time interval. Clearly, these records are not available for calculating the daily fragility forecasts. According to this Figure, the first excursion of the SD threshold is triggered by the 4th record (an event with $M = 5.3$). As it can be

[7] The time window between 6:00 UTC 07/04/09 until 6:00 UTC 08/04/09.
[8] By doing a back analysis on the sequence.

observed, the forecasted fragility curves (both ETAS and MO), predict that the limit state is going to be exceeded with probability 1 at $S_a(T)$ close to 0.14g.

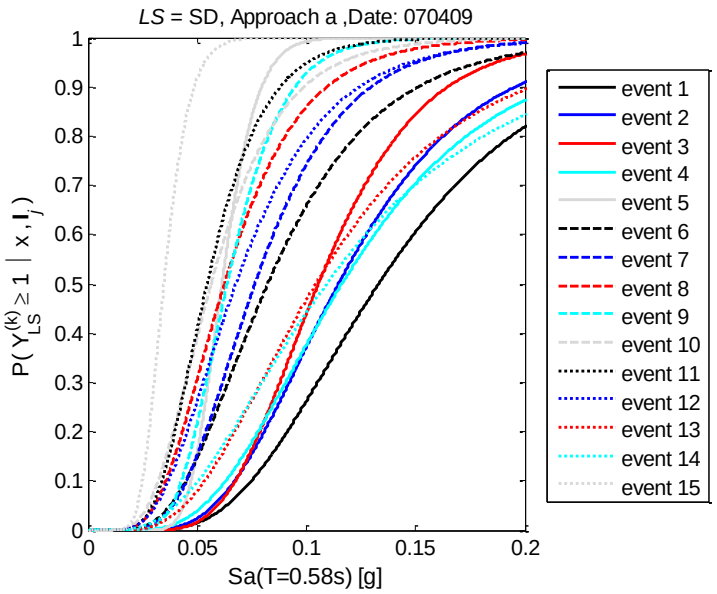

Figure 5: The sequence of fragility curves associated with Equation (17), approach "a", for day 07/04/09

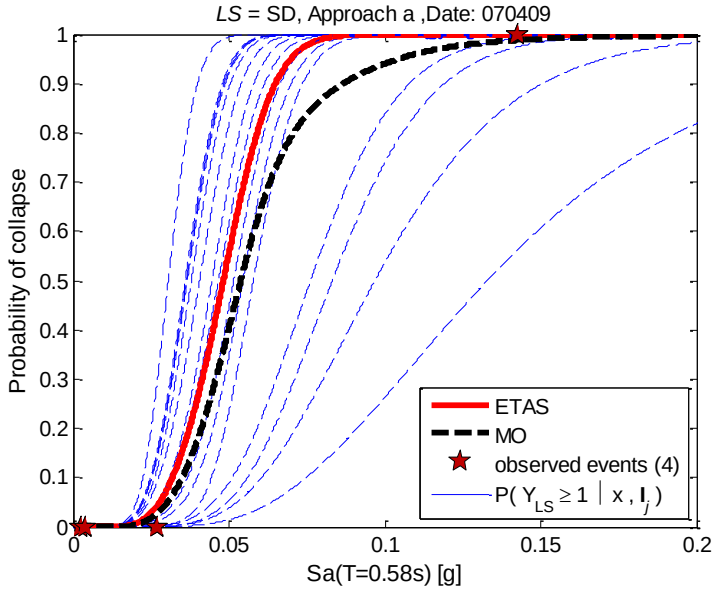

Figure 6: Forecasted fragility curves, based on both ETAS and MO models, approach "a", for day 07/04/09

4.6.1 *Comparison of daily fragility curves based on permutation and cloning*

Figure 7 illustrates the forecasted daily fragilities for SD and NC limit states for the first four days (j=1:4). It is important to note that the daily forecasts for any prescribed limit state are provided up to the day in which the first limit state excursion takes place. For example, the results for SD are only reported for the first two days elapsed after the main event (first excursion for SD takes place in the second day). These fragility curves are calculated through the first two record selection strategies (a) and (b) outlined in Section 4.5, namely, based on per-

mutation (black lines) and cloning (red lines) of aftershock records registered in **seq**, based on ETAS (solid lines) and MO (dashed lines) models.

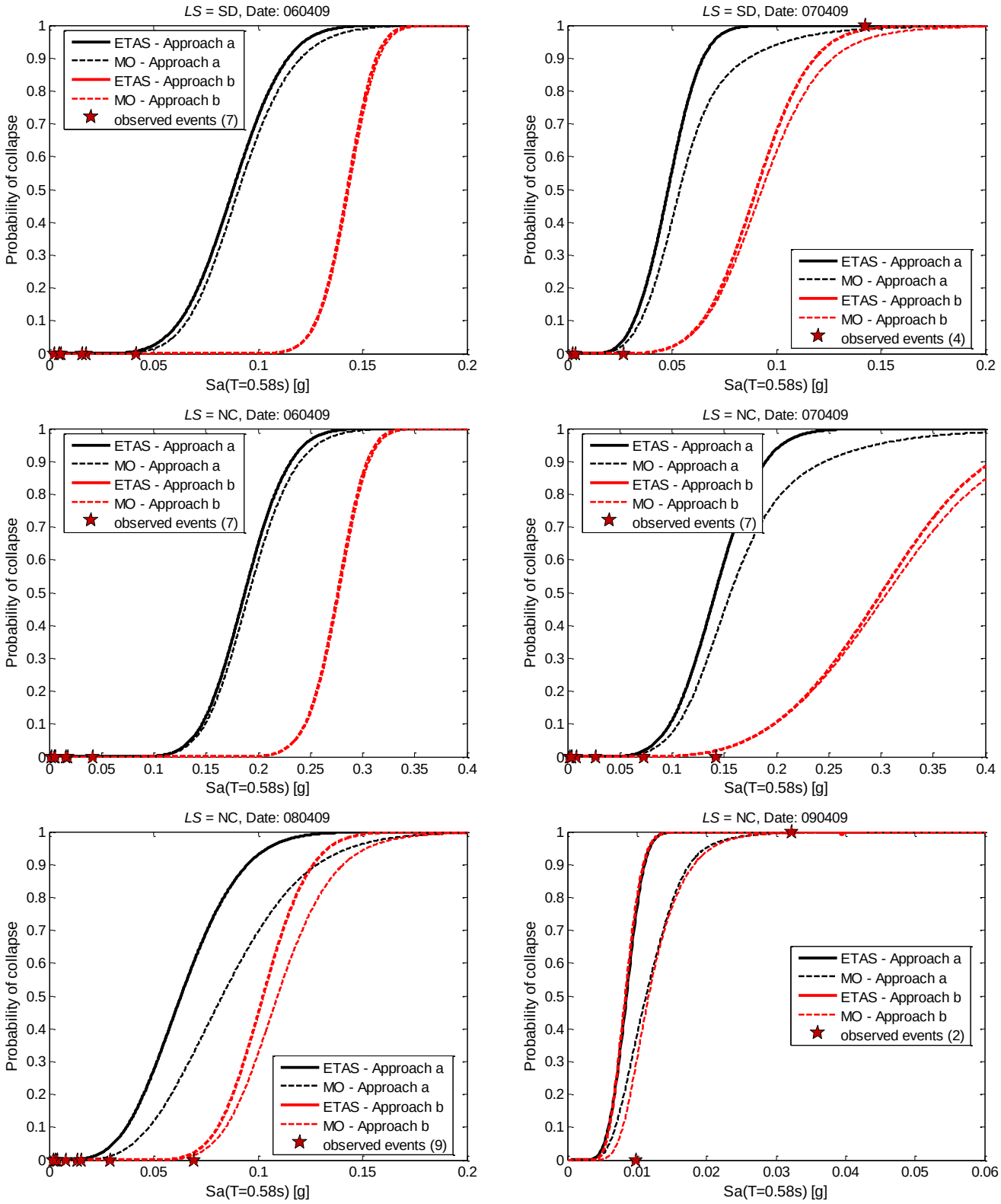

Figure 7: Forecasted daily fragility curves for the first four days, and both SD and NC limit states, based on ETAS (solid lines) and MO (dashed lines); ground motion selections strategy "a" (black lines), and "b" (red lines)

It can be depicted that the daily fragility curves based on cloning of the aftershock events are generally lower than those calculated based on permutation. This can be explained by the fact that the majority of the aftershock events are quite weak and the sequence generated by cloning them will be quite weak. Such a sequence, may fail to emulate the gradual increase in residual displacements in a real aftershock sequence. In this sense, the permutation strategy seems to provide a more realistic picture of the accumulation of damage due to a sequence of events with different magnitudes.

However, it should be kept in mind that the generated sequence $\mathbf{seq}_{\text{gen}}$ is created by selecting the previous registrations within the $\mathbf{seq}$. Given the time-dependent decreasing trend in the aftershock sequence, the permutation strategy may over-estimate the damage[9]. It is also observed that the daily fragility curves based on permutation and cloning in the fourth day are quite close. This can be attributed to the fact that the structure is very close to the onset of the limit state. This will make it vulnerable even to weaker aftershock sequences.

Discussion: From the engineering point of view, the forecasted fragility curves obtained through permutation seem to provide more robust predictions of the accumulation for residual damage in the structure. For instance, take the second-day event with local magnitude of 5.3 and $S_a\left(0.58\text{s}\right)=0.143g$ that causes the first SD limit state excursion. This is a key aftershock event which stimulates further residual deformations pushes the structure closer to the onset of NC limit state. It can be detected that the fragility curves (permutation strategy based on both ETAS and MO) predict NC first-excursion with probabilities ranging from 40% (MO) to around 50% (ETAS). This is true also for the third-day 5.1 magnitude aftershock event with $S_a\left(0.58\text{s}\right)=0.07g$ that leads to further accumulation of residual deformations and takes the structure even closer to the onset of NC. The fragility curve obtained through permutation predicts the NC first-excursion with probability 60% (ETAS-based). This is while fragility curve obtained through cloning predicts NC first-excursion with a small probability (around 2%).

4.6.2 *The daily fragility curves based on ETAS and MO methods*

Figure 8 illustrates the decrease in the structural vulnerability for DS (the first two days) and NC (the first four days) based on ETAS and MO models, adopting the permutation strategy, i.e. approach "a" in Section 4.5. It can be observed that the fragility curves obtained based on the two aftershock occurrence models are significantly different. The effect of the aftershock model on fragility estimation manifests itself through the probability distribution $P\left(n\,|\,\mathbf{I}_j\right)$. As demonstrated in Figure 4 (Section 4.4), the probability distributions $P\left(n\,|\,\mathbf{I}_j\right)$, built based on the two aftershock models ETAS and MO are quite different. As it was mentioned in Section 4.4, the ETAS model assigns zero probability to the event-dependent fragilities for n=0 to 5 ~10. Consequently, the ETAS model systematically shifts the probability content towards larger number of aftershocks per day. This means that the event-dependent fragilities for larger n are going to have a larger weight. This manifests itself into systematically larger fragility predictions based on ETAS compared to MO.

[9] In general, a stronger suite of records may manifest different frequency content characteristics with respect to the weaker records. As far as it concerns the cloud method, the domain of regression (i.e., the range of spectral acceleration values) is going to be shifted towards larger spectral acceleration values.

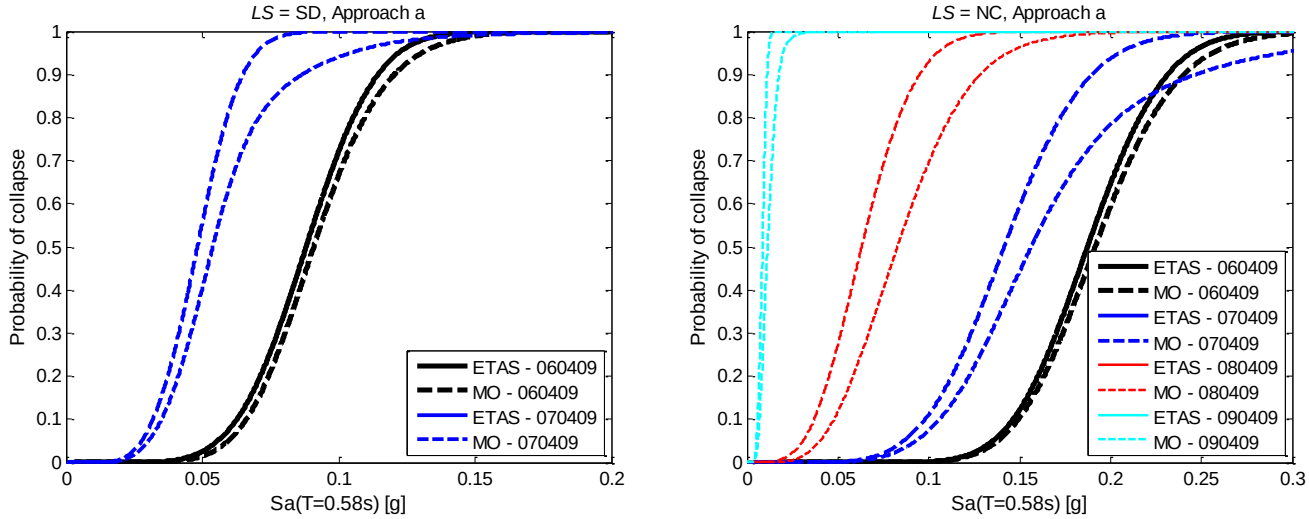

Figure 8: Forecasted daily-fragility curves (based on ETAS and MO models) for the first four days, and both for SD and NS limit states, ground motion selections strategy "a" (permutation)

4.6.3 *The daily fragility curves based on scaled strong motion recordings*

It is interesting to investigate if adopting a set of scaled ground motion records (instead of the registered aftershock records) as per [1, 12-13]) would also lead to reasonable results. In fact, this issue is addressed through strategies (c) and (d) for generating $\mathbf{seq}_{\text{gen}}$, outlined in Section 4.5. This simplifies the application of sequential cloud since it does not rely on after-shock records from the same sequence. Herein, a set of 15 European ground motion records ($N_{\text{seq}} = 15$) are chosen [5]. As mentioned in Section 4.5, these strong motion records are cloud-scaled so that their median spectral acceleration is equal to that of the ground motions within **seq**. Figure 10 illustrates the ETAS-based daily fragility curves (strategy (c): permutation, dashed lines) for limit states NC (first four days) and SD (first two days) compared to those based on strategy (a) (solid lines).

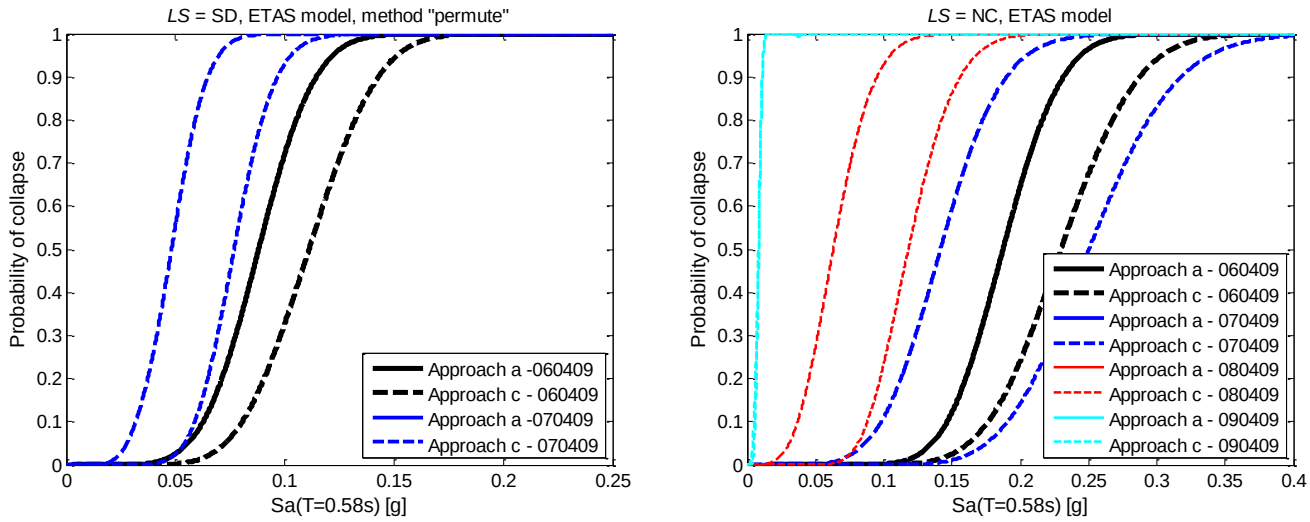

Figure 9: Forecasted daily fragility curves (ETAS) through strategy (a) and strategy (c) for SD (left) and NC (right) limit states

It can be observed that using the scaled strong motions systematically under-estimates the fragilities. This may be attributed to the change in the frequency content of the strong- and weak-motion records.

4.7 Daily aftershock risk forecasting

In this section daily aftershock risk, expressed in terms of the mean daily rate of exceeding limit states *SD* and *NC*, is calculated. This is done by the integration of the corresponding daily fragility and hazard curves. Figure 10 below illustrates the forecasted daily aftershock hazard curves, expressed in terms of mean daily rate of exceeding various levels of $S_a(0.58\text{s})$, denoted as $\lambda(x|\mathbf{I}_j)$ in Equation (7), for $3.3 \le M \le 7.5$ within the first four days after the main event (PASHA, see [11] for more details). It is should be noted that the parameters of the MO model (labeled as *seq-based*) as well as the ground motion prediction relation (Sabetta and Pugliese [25], labeled as *updated SP96*) are updated daily based on the L'Aquila sequence. In contrast to ETAS model hazard curves (solid lines) which take into account the spatio-temporal evolution of seismicity, the MO hazard curves (dashed lines) are based on the assumption of uniform seismicity in the aftershock zone (labeled as *uniform*). It can be seen that the ETAS-based hazard curves are larger than the MO-based ones, especially in the first few days elapsed after the main event. This is in line with the corresponding predictions for the number of events in Figure 4.

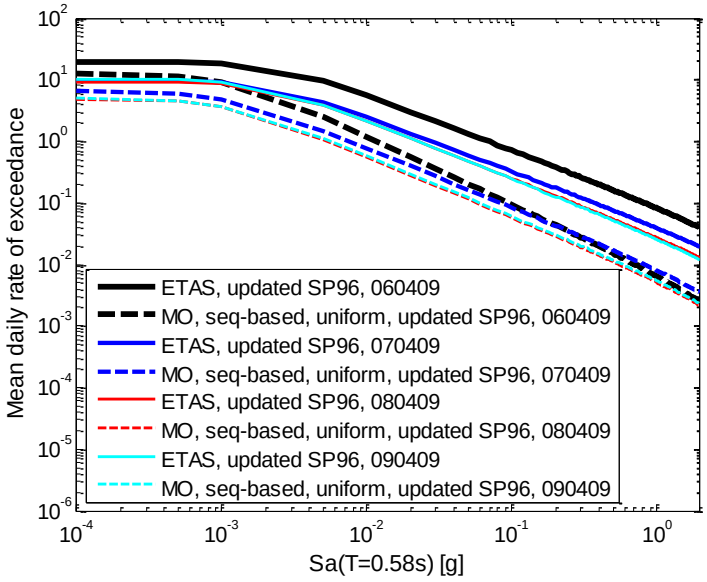

Figure 10: The mean daily rate of exceeding various levels of S_a(0.58s) based on MO and ETAS from 06/04/09 up to 09/04/09

Figure 12 illustrates the daily risk forecasts for two limit states SD and NC. The left-most column represents the ETAS-based results and the right-most column is dedicated to the MO-based results. The risk estimates obtained through strategies (a), (b), (c) and (d) are plotted as circles (black), squares (blue), triangles (red) and stars (cyan), respectively. The following observations can be made:

- The difference between the daily risk predictions based on MO and ETAS models arises from both the difference in the daily fragility and hazard forecasts. The MO model leads to systematically lower values.

- As it can be seen, the first-excursion of NC limit state in the fourth day is accurately predicted by both models. Both models predicts first-excursion of NC between during between day 3 and day 4 (i.e., when the mean day rate is equal to 1/day).
- On the other hand, the first-excursion of SD limit state is not signaled as accurately. The ETAS model (strategy (a)) predicts the risk around 0.65/day (sufficiently alarming); meanwhile the MO model (strategy (a)) predicts the risk around 0.20/day. This under-estimation can be attributed to the hazard forecasting. That is, in the second day elapsed after the main event, another seisimo-genetic structure became active and none of the two models managed to predict the hazard very well for this particular day (although ETAS did better than MO).
- The risk predictions based on ETAS method reveal higher sensitivity to the sequential cloud analysis strategies compared to MO model. In general, the strategy (a), which is based on selecting records from the ongoing sequence and generating the sequence by permutation, lead to the highest risk estimates.

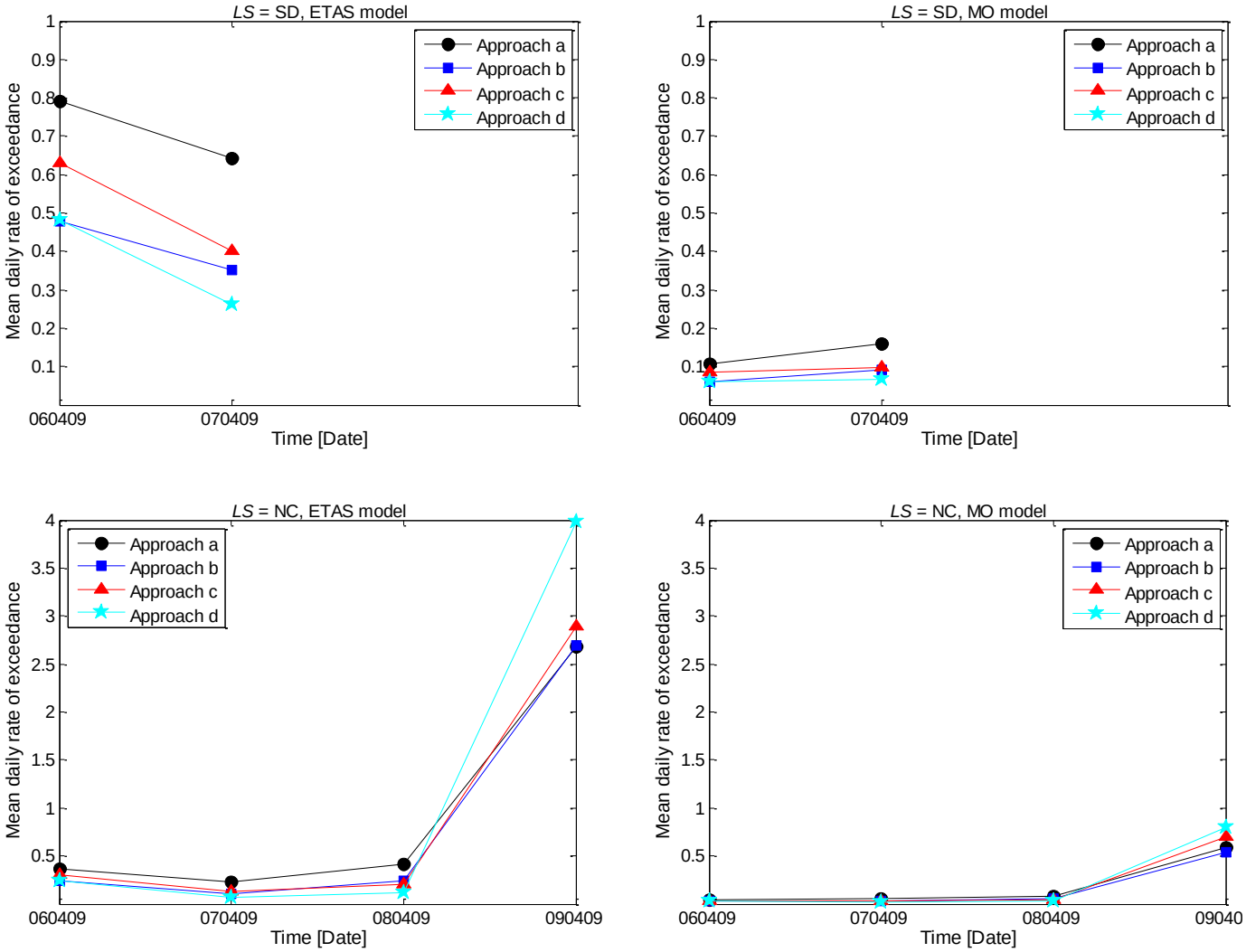

Figure 12: Daily risk forecasting for SD (upper-most row) and NC (lower-most row) limit states for the first four days from 06/04/09 to 09/04/09 based on ETAS (left-most column) and MO (right-most column)

5 CONCLUSIONS

This paper explores the various issue related to performance-based time-dependent vulnerability assessment in the presence of an ongoing aftershock sequence. This is done in the framework of operation aftershock risk forecasting. Arguably, operational risk forecasting provides a quantified support basis for rapid decision making the immediate post main event environment. The structural vulnerability in such a framework can be represented by daily fragility curves, conditional first-excursion probabilities given seismic intensity, for prescribed structural limit states. The performance objective for each limit state is defined through adoption of a novel structural performance variable. This variable is defined as the time-dependent ratio of maximum demand increment to residual limit state capacity and is equal to unity at the onset of the limit state in consideration.

An existing time-dependent risk assessment methodology proposed in [5] and [20] is modified and improved in order to construct the daily fragility curves. In this methodology, the daily fragility curves are calculated as a weighted sum of event-dependent fragility curves (the conditional first-excursion probability given that exactly *n* events have taken place). The weights are equal to the probability that exactly *n* aftershock events take place in each given day. This probability distribution is constructed based on two established aftershock recurrence models, namely, Epidemic Type Aftershock Sequence (ETAS) and Modified Omori (MO). The event-based fragility curves are calculated next through a recursive formulation as the sum of a sequence of probabilities that the first-excursion takes place after the occurrence of a certain event (within the *n* events). A non-linear dynamic analysis procedure entitled sequential cloud analysis is developed in order to calculate the latter sequence of first-excursion probabilities. In this method, the record sequence selection/generation is done by adopting four different strategies: (a) generation of a sequence by permutation of aftershock events registered previously in the ongoing sequence; (b) generation of a sequence by back-to-back repeating (cloning) of aftershock events registered previously in the ongoing sequence; (c) generation of a sequence by permutation of cloud-scaled strong motion records; (d) generation of a sequence by cloning of cloud-scaled strong motion records.

Finally, daily risk predictions, expressed in terms of the mean daily rate of limit-state first-excursion, are calculated by integrating daily hazard and fragility predictions. The daily hazard predictions are furnished from a previous work of the authors [11]. In general, the following observations can be made with regard to the case-study application demonstrated for the L'Aquila 2009 seismic sequence:

- The daily fragility predictions are quite sensitive to both the underlying aftershock model and the alternative sequence generation strategies. Overall, it seems that adopting ETAS as the underlying aftershock model and sequence generation by permutation of previous events within the ongoing sequence (strategy a) lead to the best estimates. The structural response to the real sequence is used as a benchmark for comparison.
- In particular, the probability distributions for the number of aftershock events per day, which are used as weights in the calculation of daily fragilities, significantly affect the results.
- For the example SDOF system studied herein, risk forecasting based on both ETAS and MO models manages to capture the first-excursion of near collapse NC limit state in the fourth day elapsed after the main event.
- However, for the limit state of severe damage SD neither of the two methods can provide accurate estimates of risk in the second day (although both methods signal a critical situa-

tion). This can be attributed to the short-coming of both methods in predicting the seismic hazard in the second day, due to the activation of a second fault structure.

As a final word for near future developments, it would be interesting to apply the present methodology for a range of generic SDOF and MDOF structural models in order to gain a better insight into the factors that affect the time-dependent fragility assessment in the presence of an ongoing seismic sequence.

REFERENCES

[1] Q. Li, B.R. Ellingwood, Performance evaluation and damage assessment of steel frame buildings under main shock-aftershock sequences. *Earthquake Engineering and Structural Dynamics*, **36**, 405-427, 2007.

[2] G.L. Yeo, C.A. Cornell, Post-quake decision analysis using dynamic programming. *Earthquake Engineering and Structural Dynamics*, **38**, 79-93, 2009.

[3] G.L. Yeo, C.A. Cornell, Equivalent constant rates for post-quake seismic decision making. *Structural Safety*, **31**, 443-447, 2009.

[4] K. Goda, C.A. Taylor, Effects of aftershocks on peak ductility demand due to strong ground motion records from shallow crustal earthquakes. *Earthquake Engineering and Structural Dynamics*, **41**(15), 2311-2330, 2012.

[5] F. Jalayer, D. Asprone, A. Prota, G. Manfredi, A decision support system for post-earthquake reliability assessment of structures subjected to aftershocks: an application to L'Aquila earthquake, 2009. *Bulletin of Earthquake Engineering*, **9**(4), 997-1014, 2011.

[6] J.R. Benjamin, C.A. Cornell, *Probability, statistics and decision for civil engineers*. McGraw Hill, 684pp, 1970.

[7] C.A. Cornell, F. Jalayer, R.O. Hamburger, D.A. Foutch, Probabilistic Basis for the 2000 SAC Federal Emergency Management Agency Steel Moment Frame Guidelines. *ASCE Journal of Structural Engineering*, **128**, 526-533, 2002.

[8] Y. Ogata, Statistical models for earthquake occurrences and residual analysis for point processes. *Journal of the American Statistical Association*, **83**, 9-27, 1988.

[9] W. Marzocchi, A.M. Lombardi, Real-time forecasting following a damaging earthquake, *Geophysical Research Letters*, **36**, L21302, 2009, doi 10.1029/2009GL040233.

[10] T. Utsu, A statistical study of the occurrence of aftershocks. *Geophysical Magazine*, **30**, 521-605, 1961.

[11] H. Ebrahimian, F. Jalayer, D. Asprone, A.M. Lombardi, W. Marzocchi, A. Prota, G. Manfredi, Adaptive Daily Forecasting of Seismic Aftershock Hazard. *Bulletin of Seismological Society of America*, **submitted**.

[12] N. Luco, P. Bazzurro, C.A. Cornell, Dynamic versus static computation of the residual capacity of mainshock-damaged building to withstand an aftershock. In: *Proceedings 13th World Conference on Earthquake Engineering*, Vancouver, B.C., Canada, August 1-6, 2004, Paper No. 2405.

[13] J. Ruiz-García, J.C. Negrete-Manriquez, Evaluation of drift demands in existing steel frames under as-recorded far-field and near-fault mainshock–aftershock seismic sequences. *Engineering Structures,* **33**, 621-634, 2011.

[14] J. Ruiz-García, E. Miranda, Probabilistic estimation of residual drift demands for seismic assessment of multi-story framed buildings. *Engineering Structures,* **32**, 11-20, 2010.

[15] J. Ruiz-García, J.Y. Moreno, I.A. Maldonado, Evaluation of existing Mexican highway bridges under mainshock–aftershock seismic sequences. In: *Proceedings of the 14th World Conference on Earthquake Engineering*, Beijing, China, October 12-17, 2008, Paper No. 05-02-0090.

[16] G.D. Hatzigeorgiou, A.A. Liolios, Nonlinear behaviour of RC frames under repeated strong ground motions. *Soil Dynamics and Earthquake Engineering*, **30**, 1010-1025, 2010.

[17] F. Jalayer, P. Franchin, P.E. Pinto, A scalar damage measure for seismic reliability analysis of RC frames. *Earthquake Engineering and Structural Dynamics*, **36**, 2059-2079, 2007.

[18] Y. Ogata, Space-time point-process models for earthquake occurrences. *Annals of the Institute of Statistical Mathematics*, **50** (2), 379-402, 1998.

[19] H. Ebrahimian, F. Jalayer, D. Asprone, A.M. Lombardi, W. Marzocchi, A. Prota, G. Manfredi, Adaptive post-earthquake reliability assessment of structures subjected to aftershocks. *11th International Conference on Structural Safety & Reliability (ICOSSAR 2013*), Columbia University, New York, NY, June 16-20, 2013.

[20] F. Jalayer, D. Asprone, A. Prota, G. Manfredi, Multi-hazard upgrade decision making for critical infrastructure based on life-cycle cost criteria. *Earthquake Engineering and Structural Dynamics*, **40**(10), 1163-1179, 2011.

[21] E.T. Jaynes, *Probability Theory: The Logic Of Science*. Cambridge University Press, 2004.

[22] F. Jalayer, C.A. Cornell, A Technical Framework for Probability-Based Demand and Capacity Factor Design (DCFD) Seismic Formats. *Pacific Earthquake Engineering Center* (*PEER*) 2003/08, November 2003.

[23] CEN. *Eurocode 8: design of structures for earthquake resistance. Part 3: assessment and retrofitting of buildings.* EN 1998-3, CEN, Brussels, March 2005.

[24] D. Asprone, F. Jalayer, A. Prota, G. Manfredi, Proposal of a probabilistic model for multi-hazard risk assessment of structures in seismic zones subjected to blast for the limit state of collapse. *Structural Safety* **32**(1), 25-34, 2010.

[25] F. Sabetta, A. Pugliese, Estimation of response spectra and simulation of nonstationary earthquake ground motions. *Bulletin of Seismological Society of America*, **86**(2), 337-352, 1996.